# Output Power Characteristics of Isolated Secondary-Resonant SAB DC-DC Converter for Output Voltage Variation

Shota Yamashita, Kohei Budo, Takaharu Takeshita
Dept. of Electrical and Mechanical Engineering, Graduate School of Engineering
Nagoya Institute of Technology
Gokiso, Showa, Nagoya
Aichi, 466-8555 Japan
Tel.: +81 / (52) 735 – 5441
Fax: +81 / (52) 735 – 5432
E-Mail: take@nitech.ac.jp
URL: http://motion.web.nitech.ac.jp/

## Acknowledgements

A part of this work was supported by JSPS KAKENHI Grant Number JP21H01310.

## Keywords

«DC-DC converter», «Isolated converter», «High frequency power converter», «Soft switching», «Dual Active Bridge (DAB)»

## Abstract

The Secondary-Resonant Single Active Bridge (SR-SAB) converter is proposed as a high power, low-cost, compact, and high-efficiency DC-DC converter. The SR-SAB converter is composed of the H-bridge circuit, the high-frequency transformer, and the diode rectifier circuit with resonant capacitors connected in parallel. When primary H-bridge circuit switches, the resonant capacitors cause LC resonance. Due to LC resonance, the secondary diode rectifier circuit switching is delayed and the secondary voltage is lags behind the primary voltage like the DAB converter. While LC resonance occurs, large voltage is applied to leakage inductance and secondary current increase significantly. Therefore, the SR-SAB converter achieves high total power factor like DAB converter with simple SAB converter circuit. This paper presents the output power characteristics of the SR-SAB converter for the output voltage variation. The effectiveness of output power characteristics for output voltage variation of the SR-SAB converter is verified by experiments.

## Introduction

The electric vehicle (EV) is attracting public attentions to solve environmental problems. The compact and high-efficiency isolated DC-DC converter is needed for EV's battery charger [1]. The bidirectional isolated Dual-Active-Bridge (DAB) DC-DC converter has been proposed. Fig.1 shows the DAB converter. Fig.2 shows the conventional SAB converter. Fig.3 shows the SR-SAB converter. The DAB converter is composed of H-bridges on the primary and secondary side and high-frequency transformer [2], [3]. Fig.4 shows waveforms of the DAB converter, the conventional SAB converter and the SR-SAB converter. Square waves of the primary voltage $v_1$ and secondary voltage $v_2$ are generated by controlling H-bridge circuits. The DAB converter transforms the power using phase difference between the primary voltage $v_1$ and the secondary voltage $v_2$. While the secondary voltage $v_2$ lags behind the primary voltage $v_1$, the leakage inductance voltage $v_L$, the voltage applied to the leakage inductance, is difference of the primary voltage $v_1$ and the secondary voltage $v_2$ (= sum of the input DC voltage $V_{in}$ and the output DC voltage $V_{out}$), the secondary current $i_2$ increases significantly. Therefore, the DAB converter achieves high total power factor and the DAB converter can transform power even if the input DC voltage $V_{in}$ is lower than the output DC voltage $V_{out}$. By controlling the phase between the

primary voltage $v_1$ and the secondary voltage $v_2$, the DAB converter achieves output power control and bidirectional power transformation [4], [5]. The simple and low-cost isolated DC-DC converter compared with DAB converter is needed for unidirectional power conversion such as battery charger.

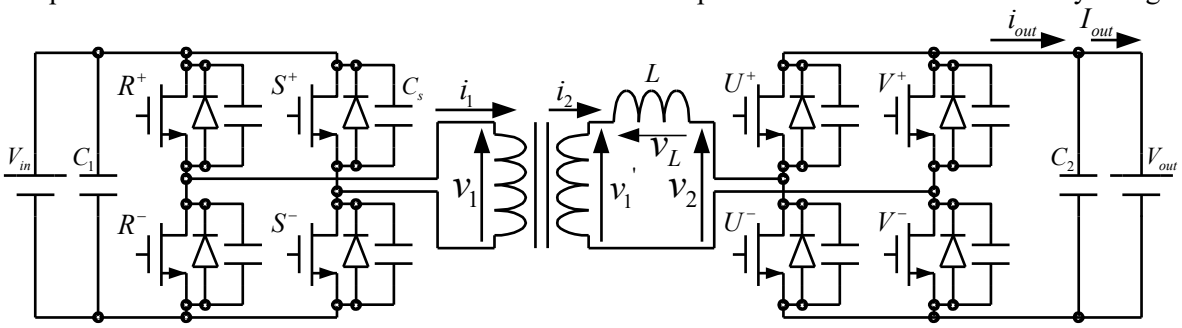


Fig. 1 : Conventional DAB converter circuit configuration

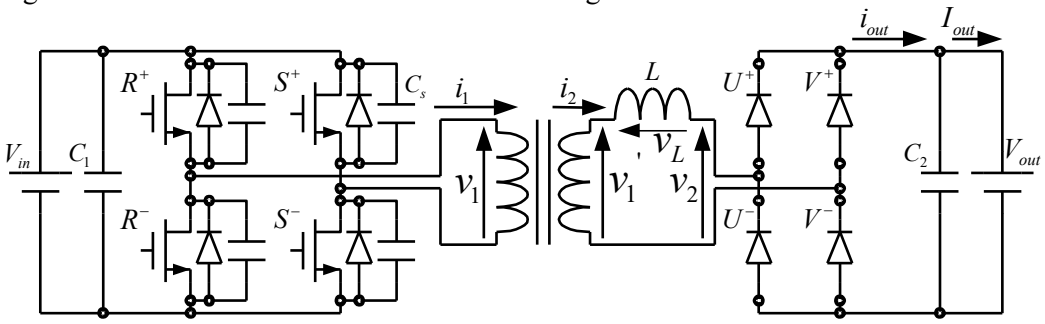


Fig. 2 : Conventional SAB converter circuit configuration

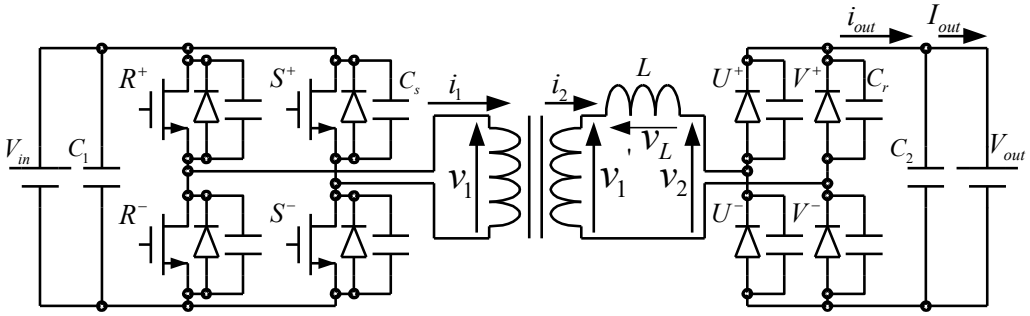


Fig. 3 : Proposed SR-SAB DC-DC converter circuit configuration

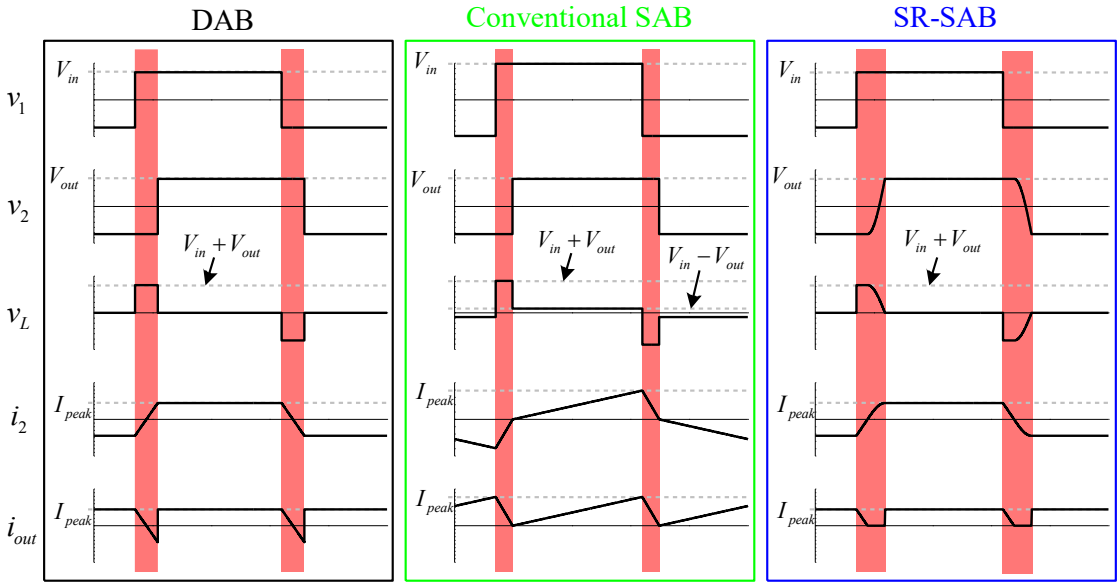


Fig. 4 : Waveforms of the DAB converter, the conventional SAB converter and the SR-SAB converter

The unidirectional isolated Single-Active-Bridge (SAB) DC-DC converter has been proposed. The SAB converter is composed of the H-bridge circuit, high-frequency transformer and the diode rectifier circuit [6],[7],[8]. The SAB converter is a low-cost and compact unidirectional isolated DC-DC converter. Square wave of the primary voltage $v_1$ is generated by controlling H-bridge circuit. The secondary voltage $v_2$ depends on on/off state of the secondary diodes. The phase difference between the primary voltage $v_1$ and the secondary voltage $v_2$ is short and the secondary current $i_2$ dose not increase sufficiently. Therefore, total power factor of the conventional SAB converter is low compared with the DAB converter.

The authors have proposed a high power, low-cost, compact, and high-efficiency isolated Secondary-Resonant SAB (SR-SAB) DC-DC converter [9][10][11]. The SR-SAB converter is composed of the H-bridge circuit on the primary side and the diode rectifier circuit with resonant capacitors connected in parallel on the secondary side. Because the resonant capacitors delay turn-on of diodes of the secondary rectifier circuit, the secondary voltage $v_2$ lags behind the primary voltage $v_1$. By the delay of the primary voltage $v_1$, the voltage applied to leakage inductor $v_L$ is difference of the primary voltage $v_1$ and the secondary voltage $v_2$ and the secondary current $i_2$ increases significantly like the DAB converter. Therefore, the SR-SAB converter achieves high total power factor, like the DAB converter, with simple circuit configuration like the conventional SAB converter.

This paper presents the analysis and the output power characteristics of the SR-SAB converter for the output DC voltage $V_{out}$ variation. The output power of the proposed SR-SAB converter can be expressed by using only four-points in the secondary current $i_2$. First, the secondary current $i_2$ waveform of the SR-SAB converter is derived by considering the behaver of the secondary side. Next, the output power characteristics for output DC voltage $V_{out}$ variation of the SR-SAB converter is derived by using secondary $i_2$ current waveform. Finally, the effectiveness of the output power characteristics is verified by comparing the experimental results with theoretical characteristics.

# Overview of the SR-SAB Converter

## Waveform of the SR-SAB and the conventional SAB converter

Table 1 shows condition of the waveform of the waveforms of the conventional SAB converter and the SR-SAB converter. In the conventional SAB converter, the primary voltage $v_1$ with the amplitude as the input DC voltage $V_{in}$ is generated by controlling four switches $R^+$, $R^-$, $S^+$, and $S^-$. The secondary voltage $v_2$ is a square wave with the amplitude as the output DC voltage $V_{out}$. The secondary voltage $v_2$ is lags behind the primary voltage $v_1$. When secondary current $i_2$ reaches zero, the diodes of the secondary side turns-on, and the secondary voltage $v_2$ switches and the phase delay period shown in red in the Fig.4 (the period between switching of the primary voltage $v_1$ and switching of the secondary voltage $v_2$) finishes. The leakage inductance voltage $v_L$ is difference of the secondary voltage $v_2$ minus the primary voltage $v_1$. Sum of the input DC voltage $V_{in}$ and the output DC voltage $V_{out}$ is applied to the leakage inductance voltage $v_L$ during the phase delay period and difference of input DC voltage $V_{in}$ minus the output DC voltage $V_{out}$ is applied during the other periods. The secondary current $i_2$ increases by the leakage inductance voltage $v_L$. The secondary current $i_2$ increases significantly during the phase delay period and increases slowly during the other period. Because the phase delay period is short, the secondary current $i_2$ dose not increase sufficiently. Therefore, total power factor of the conventional SAB converter is low. The output current $i_{out}$ is the rectified secondary current $i_2$.

The condition of waveforms in Fig.4 is shown in Table 1. In the SR-SAB converter, the primary voltage $v_1$ with the amplitude as the input DC voltage $V_{in}$ is generated by controlling four switches $R^+$, $R^-$, $S^+$, and $S^-$. The secondary voltage $v_2$ is a square wave with sign wave-like rising edge with the amplitude as the output DC voltage $V_{out}$. The secondary voltage $v_2$ is lags behind the primary voltage $v_1$. When secondary current $i_2$ reaches zero, resonant capacitors $C_r$ start discharging by the secondary LC resonance between leakage inductor $L$ and resonant capacitors $C_r$ of secondary side. While the secondary LC resonance occurs, resonance capacitors $C_r$ have charge, therefore, the diodes of the secondary side are off state and the secondary voltage $v_2$ rises with sign wave-like rising edge. When

resonance capacitors $C_r$ finish discharging, the secondary LC resonance finishes and the phase delay period shown in red in the Fig.4 finishes. This means that the phase delay period is extended by the secondary LC resonance. The leakage inductance voltage $v_L$ is difference of the secondary voltage $v_2$ minus the primary voltage $v_1$. During the phase delay period, large voltage is applied to the leakage inductance voltage $v_L$ and during the other period, difference of input DC voltage $V_{in}$ minus the output DC voltage $V_{out}$ is applied. The secondary current $i_2$ increases by the leakage inductance voltage $v_L$. The secondary current $i_2$ increases significantly during the phase delay period. Because the phase delay period is extended by the secondary LC resonance, the secondary current $i_2$ increase sufficiently. Therefore, total power factor of the SR-SAB converter is high. During the secondary LC resonance period, the secondary current $i_2$ flow only resonant capacitors $C_r$ and transformer, therefore, the output current $i_{out}$ is zero during the secondary LC resonance period and the output current $i_{out}$ is the rectified secondary current $i_2$ during the other period.

Table 1 shows parameters of the SR-SAB converter and the conventional SAB converter. The peak current $I_{peak}$ is the peak current the secondary current $i_2$. The peak current $I_{peak}$ of the SR-SAB converter is lower than the conventional SAB converter. Total power factor of the SR-SAB converter is higher than the conventional SAB converter.

## Characteristics of the SR-SAB for output voltage variation

Fig.5 shows the operating waveforms of the SR-SAB converter under $V_{in} = V_{out}$ condition as black line, under $V_{in} > V_{out}$ condition as red dashed line, under $V_{in} < V_{out}$ condition as blue dashed line, restrictively.

Table 1 : Parameters of the SR-SAB converter and the conventional SAB converter

| | SR-SAB converter | Conventional SAB converter |
|---|---|---|
| Input DC voltage $V_{in}$ | 265 V | 345 V |
| Output DC voltage $V_{out}$ | 265 V | 265 V |
| Output power $P_{out}$ | 2.5 kW | 2.5 kW |
| Leakage inductance $L$ | 92 uH | 92 uH |
| Resonant capacitor $C_r$ | 43 nF | - |
| Frequency of transformer $f$ | 20 kHz | 20 kHz |
| Peak current $I_{peak}$ | 11.5 A | 19.2 A |
| Total power factor | 0.92 | 0.67 |

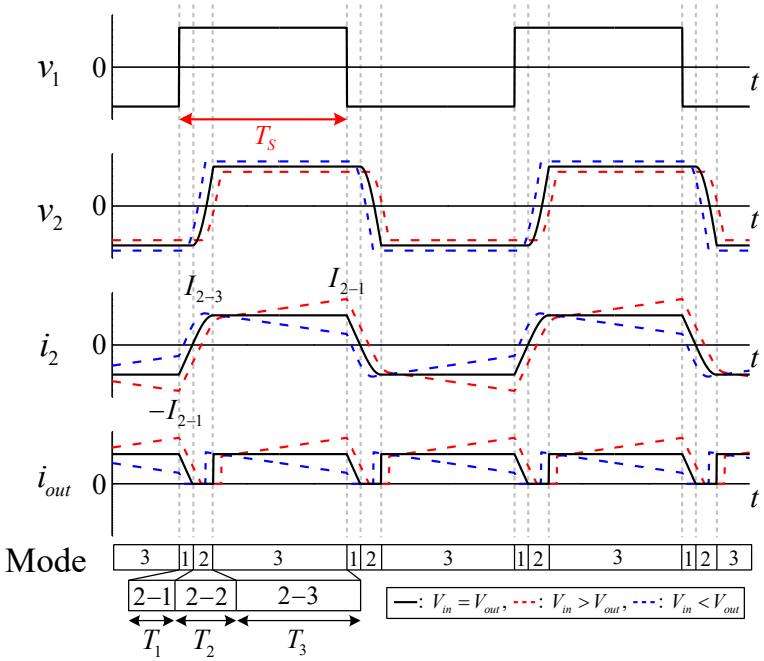


Fig. 5 : Operating waveform of the SR-SAB converter

The operation of the SR-SAB converter is divided into three operation modes. The Mode 2-1 starts when the primary voltage $v_1$ switches. During the duration $T_1$ of the Mode 2-1, sum of the input DC voltage and output DC voltage is applied to the leakage inductance voltage $v_L$ and the secondary current $i_2$ increases significantly. The initial value $I_{2-1}$ is the initial value of the Mode2-1 of the secondary current $i_2$. The Mode 2-1 finishes when secondary current $i_2$ reaches zero, and the Mode 2-2 starts. During the duration $T_2$ of the Mode 2-2, the secondary LC resonance occurs and the diodes of secondary side are off state. Therefore, large voltage is applied to the leakage inductance voltage $v_L$ and the secondary current $i_2$ increases significantly. The Mode 2-2 finishes when secondary voltage $v_2$ reaches the output voltage $V_{out}$, and the Mode 2-3 starts. During the duration $T_3$ of Mode 2-3, diodes of secondary side are on state. The leakage inductance voltage $v_L$ is the input DC voltage minus the output DC voltage $V_{out}$, therefore, increase or decrease in the secondary current $i_2$ depends on the relationship between the input DC voltage $V_{in}$ and the output DC voltage $V_{out}$. The initial value $I_{2-3}$ is the initial value of the Mode 2-3 of the secondary current $i_2$. The Mode 2-3 finishes when the primary voltage $v_1$ switches again.

The red dushed waveforms in Fig.5 shows the waveforms of SR-SAB converter under $V_{in} > V_{out}$ condition. In the Mode 2-3, secondary current $i_2$ increases and the initial value $I_{2-1}$ is larger than $V_{in} = V_{out}$ condition. Because the initial value $I_{2-1}$ is larger, the duration $T_1$, period of time until secondary current $i_2$ reaches zero, is longer than $V_{in} = V_{out}$ condition. The duration $T_2$ is short and the initial value $I_{2-3}$ is small because duration of the secondary LC resonance depends on the output DC voltage $V_{out}$.

The blue dushed waveforms in Fig.5 shows the waveforms of SR-SAB converter under $V_{in} < V_{out}$ condition. In the Mode 2-3, secondary current $i_2$ decreases and the initial value $I_{2-1}$ is smaller than $V_{in} = V_{out}$ condition. Because the initial value $I_{2-1}$ is smaller, the duration $T_1$ is shorter than $V_{in} = V_{out}$ condition. The duration $T_2$ is long and the initial value $I_{2-3}$ is large because duration of the secondary LC resonance depends on the output DC voltage $V_{out}$.

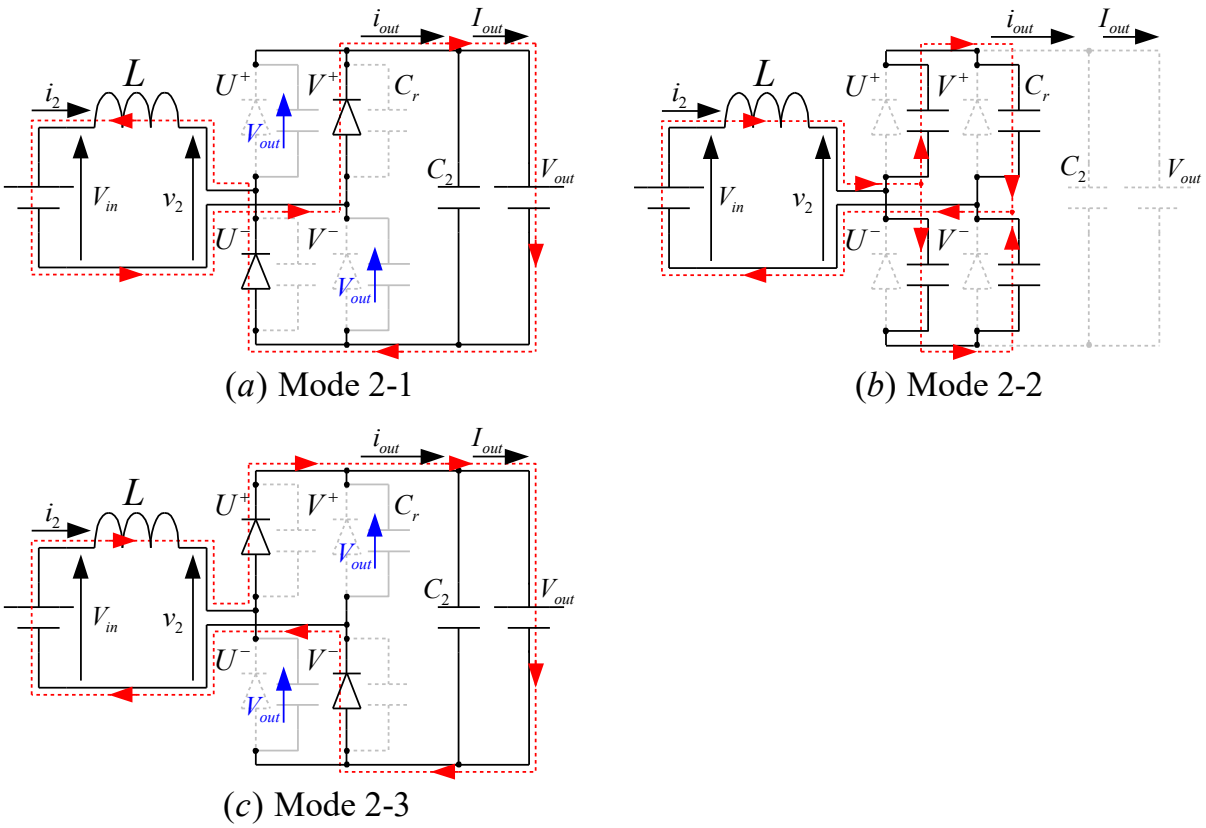


(a) Mode 2-1

(b) Mode 2-2

(c) Mode 2-3

Fig. 6 : The secondary circuit operation

## Operation Theory of Secondary-Converter

This chapter explains the operation theory of the secondary side to obtain the output power $P_{out}$ expressed by the secondary current $i_2$. Fig.6 shows the secondary connection diagrams of the Mode 2-1, the Mode 2-2, and the Mode 2-3, respectively in the Fig.5 based on the conduction pattern of secondary diodes when the primary switches $R^+$ and $S^-$ are on-state. The primary voltage $v_1$ is used as the DC voltage source because the primary switches $R^+$ and $S^-$ are on-state. In the Mode 2-1, the secondary current $i_2$ increases toward zero because the primary voltage $v_1 = V_{in}$ and the diodes $U^-$ and $V^+$ are on-state. When the secondary current $i_2$ reaches zero, all diodes on the secondary side are off-state, then the Mode 2-2 begins. In the Mode 2-2, the secondary LC resonance between leakage inductor $L$ and resonant capacitors $C_r$ occurs. All diodes of secondary side keep off-state. When the capacitor voltage connected to diode $U^+$ and $V^-$ are zero-voltage, diode $U^+$ and $V^-$ are on-state, then the Mode 2-3 begins. In the Mode 2-3, the secondary diodes $U^+$ and $V^-$ are on-state. When the primary switches $R^-$ and $S^+$ are on-state, the secondary side operates with the secondary current flowing in the reverse direction of the diagram.

Fig.6 (a) shows the secondary circuit and the flow of secondary current $i_2$ in the Mode 2-1 with red lines. In this paper, time $t = 0$ is defined as the timing of the primary voltage $v_1$ switched from $v_1 = -V_{in}$ to $v_1 = V_{in}$. The secondary current $i_2$ of the Mode 2-1 is obtained from voltage-equation of Fig.6(a) by using the initial value $i_2(0) = -I_{2-1}$ as follows:

$$i_2(t) = \frac{V_{in} + V_{out}}{L} t - I_{2-1} \qquad (0 \le t \le T_1) \tag{1}$$

$$i_{out}(t) = |i_2(t)| \qquad (0 \le t \le T_1) \tag{2}$$

The duration $T_1$ of the Mode 2-1 is obtained from $i_2(T_1) = 0$ as follows:

$$T_1 = \frac{L}{V_{in} + V_{out}} I_{2-1} \tag{3}$$

Fig.6(b) shows the secondary circuit and the flow of the secondary current $i_2$ during the Mode 2-2 with the red line. The resonant capacitor $C_r$ and the transformer leakage inductance $L$ cause the secondary LC resonance. The secondary current $i_2$ flows through the resonant capacitor $C_r$ as shown in Fig.6(b). Because the secondary current $i_2$ increases by phase difference created by the secondary LC resonance. The current flows only through the resonant capacitor, and the output current $i_{out}$ is zero. The secondary current $i_2$ of the Mode2-2 is obtained from voltage equation of Fig.6(b) by using the initial value $i_2(T_1) = 0$ and the duration $T_1$ of the Mode 2-1 as follows:

$$i_2(t) = \sqrt{LC_r}(V_{in} + V_{out}) \sin \frac{1}{\sqrt{LC_r}} (t - T_1) \qquad (T_1 \le t \le T_1 + T_2) \tag{4}$$

$$i_{out}(t) = 0 \qquad (T_1 \le t \le T_1 + T_2) \tag{5}$$

The secondary LC resonance in secondary circuit finishes when the voltage of the resonance capacitor $C_r$ of $U^-$ and $V^+$ reaches zero and diode of $U^-$ and $V^+$ turn on. Therefore, the duration $T_2$ of the Mode 2-2 is obtained as follows:

$$T_2 = \sqrt{LC_r} \cos^{-1}\left(\frac{V_{in} - V_{out}}{V_{in} + V_{out}}\right) = A \cos^{-1} \frac{\beta}{2 - \beta} \tag{6}$$

$$I_{2-3} = i_2(T_2) = 2\frac{A}{L} V_{in} \sqrt{1 - \beta} \tag{7}$$

where $A = \sqrt{LC_r}$ and $\beta = (V_{in} - V_{out})/V_{in}$.
Fig.6(c) shows the secondary circuit and the flow of the secondary current $i_2$ during the Mode 2-3 with red lines. The secondary current $i_2$ is obtained from voltage-equation of Fig.6(c) by using the initial value $i_2(T_1 + T_2) = I_{2-3}$ and the duration $T_2$ of the Mode 2-2 as follows:

$$i_2(t) = \frac{V_{in} - V_{out}}{L}(t - T_1 - T_2) + I_{2-3} \qquad (T_1 + T_2 \le t \le T_1 + T_2 + T_3) \tag{8}$$

$$i_{out}(t) = |i_2(t)| \qquad (T_1 + T_2 \le t \le T_1 + T_2 + T_3) \tag{9}$$

## Characteristics Output Power

The output power $P_{out}$ is obtained using the four-parameters $I_{2-1}$, $I_{2-3}$, $T_1$, and $T_3$ as follow:

$$P_{out} = \frac{1}{T_S}\int V_{out}\, i_{out} dt = \frac{V_{out}}{2T_S}\{(I_{2-1} + I_{2-3})T_3 + I_{2-1}T_1\}, \tag{10}$$

Where

$$T_S = T_1 + T_2 + T_3 \tag{11}$$

This chapter explains the derivation method of four parameters $I_{2-1}$, $I_{2-3}$, $T_1$, and $T_3$ of the output power $P_{out}$ in (10) to obtain the output power $P_{out}$ characteristics for the output DC voltage $V_{out}$ variation $\beta(= (V_{in} - V_{out})/V_{in})$ which means the relation between input DC voltage $V_{in}$ and output DC voltage $V_{out}$. Fig.7 shows the four parameters $I_{2-1}$, $I_{2-3}$, $T_1$, and $T_3$ on the secondary current $i_2$ in the half period $T_S$.

Because the secondary current $i_2$ cyclically changes, equations are obtained from $i_2(T_S) = -i_2(0)$ as follow:

$$i_2(T_S) = \frac{V_{in} - V_{out}}{L}(T_s - T_1 - T_2) + I_{2-3} = I_{2-1} \tag{12}$$

Parameters $T_1$, $T_3$, and $I_{2-1}$ are obtained from equations (3), (6), (7), (11), and (12)

$$T_1 = \frac{1}{2}\beta(T_S - T_2) + A\sqrt{1-\beta} \tag{13}$$

$$T_3 = \frac{1}{2}(2-\beta)(T_S - T_2) - A\sqrt{1-\beta} \tag{14}$$

$$I_{2-1} = \frac{V_{in}}{2L}(-\beta^2 + 2\beta)(T_S - T_2) + \frac{V_{in}}{L}A(2-\beta)\sqrt{1-\beta} \tag{15}$$

Because $\beta$ is close to zero, following approximation can be used.

$$(-\beta + 1)^{\frac{1}{2}} \approx 1 - \frac{1}{2}\beta \tag{16}$$

$$\cos^{-1}\frac{\beta}{2-\beta} \approx \left(\frac{\pi}{2} - \frac{1}{2}\beta\right) \tag{17}$$

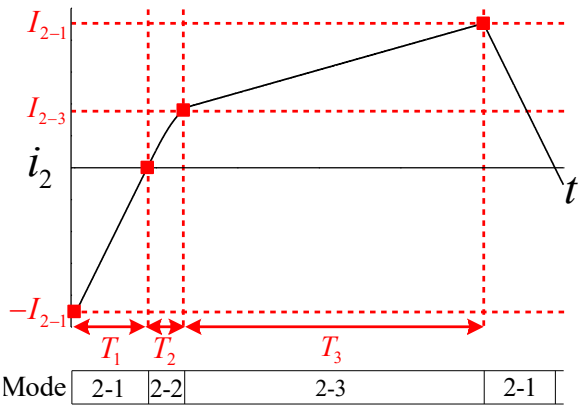


Fig. 7 : Four points of secondary current $i_2$

Parameters are simplified by applying approximation (16) and (17) to (6), (7), (13), (14), and (15) as follow:

$$T_1 \approx \frac{1}{4}A\beta^2 + \left\{\frac{1}{2}T_S - \left(\frac{\pi}{2}+\frac{1}{2}\right)A\right\}\beta + A, \tag{18}$$

$$T_2 \approx A\left(\frac{\pi}{2} - \frac{1}{2}\beta\right) \tag{19}$$

$$T_3 \approx -\frac{1}{4}A\beta^2 + \left\{-\frac{1}{2}T_S + \left(\frac{\pi}{2}+1\right)A\right\}\beta + T_S - \left(\frac{\pi}{2}+1\right)A, \tag{20}$$

$$I_{2-1} \approx \frac{V_{in}}{L}\left[-\frac{1}{4}A\beta^3 + \left\{-\frac{1}{2}T_S + \left(\frac{\pi}{4}+1\right)A\right\}\beta^2 + \left\{T_S - \left(\frac{\pi}{2}+2\right)A\right\}\beta + 2A\right] \tag{21}$$

$$I_{2-3} \approx 2\frac{A}{L}V_{in}\left(1 - \frac{1}{2}\beta\right) \tag{22}$$

The output power $P_{out}$ is derived substituting (18), (19), (20), (21), and (22) for (10) and expressed by circuit parameters $V_{in}$, $V_{out}$, $L$, $C_r$ and switching frequency $(1/2T_S)$. The output power $P_{out}$ is derived as simplified equation as follow:

$$\begin{aligned} P_{out} = \frac{{V_{in}}^2}{2T_S L}\Bigg[&\frac{1}{8}A^2\beta^5 + \left\{-\frac{1}{8}A^2 + \frac{1}{2}AT_S - \left(\frac{\pi}{4}+\frac{3}{4}\right)A^2\right\}\beta^4 \\ &+ \left\{\frac{1}{2}{T_S}^2 - \left(\frac{\pi}{2}+\frac{5}{2}\right)AT_S + \left(\frac{1}{8}\pi^2 + \frac{3}{2}\pi + \frac{13}{4}\right)A^2\right\}\beta^3 \\ &+ \left\{-\frac{3}{2}{T_S}^2 + \left(\frac{3}{2}\pi + 6\right)AT_S - \left(\frac{3}{8}\pi^2 + \frac{15}{4}\pi + \frac{13}{2}\right)A^2\right\}\beta^2 \\ &+ \left\{{T_S}^2 - (\pi+8)AT_S + \left(\frac{1}{4}\pi^2 + \frac{9}{2}\pi + 6\right)A^2\right\}\beta \\ &+ 4AT_S - (2\pi+2)A^2\Bigg] \end{aligned} \tag{23}$$

Table 2 : Experimental conditions

| | |
|---|---|
| Input DC voltage $V_{in}$ | 265 V |
| Leakage inductor $L$ | 92 μH |
| Resonant capacitor $C_r$ | 43 nF |
| Frequency of transformer $1/(2T_S)$ | 20 kHz |
| DC capacitor $C_1$,$C_2$ | 1500 μF |

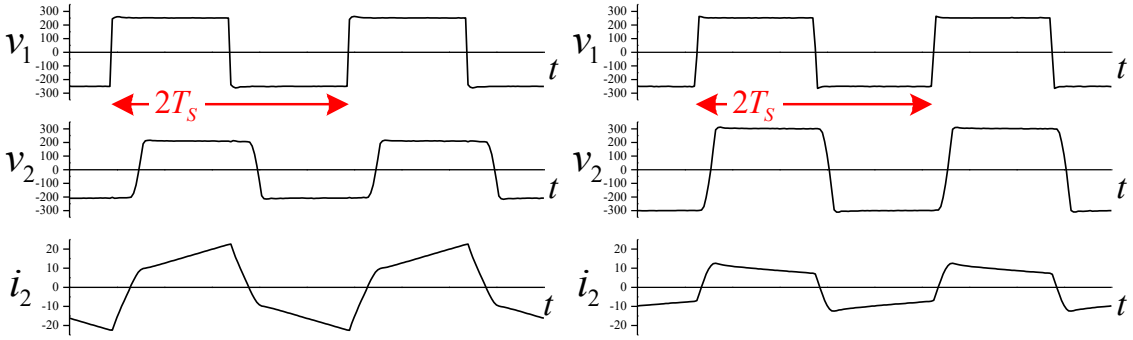


(a) $\beta = 0.245$ ($V_{out} = 200$ V) (b) $\beta = -0.0943$ ($V_{out} = 290$ V)

Fig. 8 : Experimental waveforms

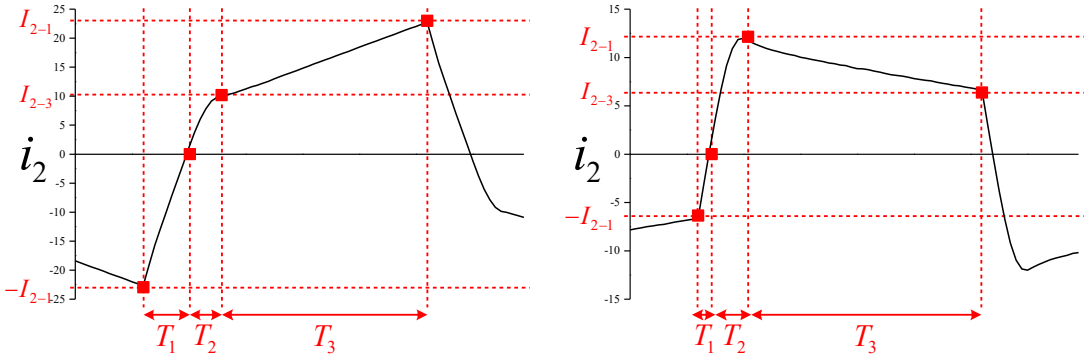


(a) $\beta = 0.245$ ($V_{out} = 200$ V) (b) $\beta = -0.0943$ ($V_{out} = 290$ V)

Fig. 9 : Experimental secondary current $i_2$ waveform for one period

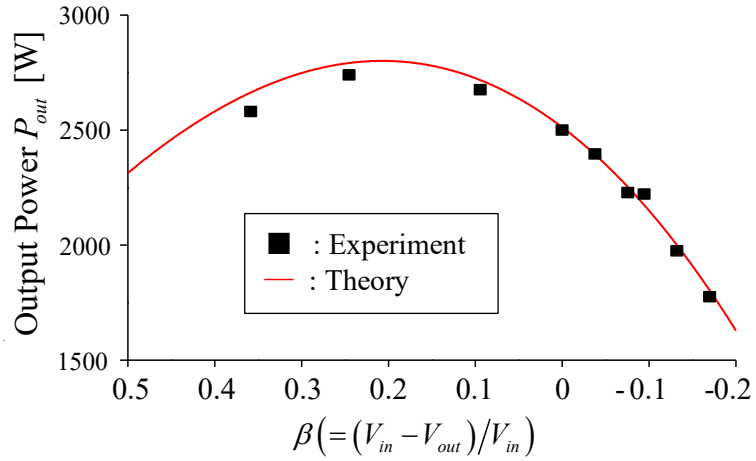


Fig. 10 : Experimental result of the output power with respect to $\beta$

## Experimental Results

Table 2 shows experimental conditions. Leakage inductor $L$ and resonant capacitor $C_r$ are designed to provide 2.5 kW output power under the output DC voltage $V_{out}$ = DC voltage $V_{in}$ condition.

Fig.8 shows the experimental waveforms under $\beta = 0.245$ ($V_{out} = 200$ V) and $\beta = -0.0943$($V_{out} = 290$ V) condition. The effective value of the secondary current $i_2$ is high under the input DC voltage $V_{in}$ > output DC voltage $V_{out}$ condition. The effective value of the secondary current $i_2$ is low under the input DC voltage $V_{in}$ < output DC voltage $V_{out}$ condition.

Fig.9 shows the experimental secondary current $i_2$ waveform for one period as black line and the theorical secondary current parameter values in equations (18), (19), (20), (21) and (22) as red square symbols. The experimental secondary current $i_2$ waveforms are agreement with the theorical secondary current $i_2$ parameter values.

Fig.10 shows the experimental result of the output power $P_{out}$ as black square symbols and the theorical output power $P_{out}$ in equation (23) as a red line. The experimental output power $P_{out}$ characteristics are agreement with theorical output power $P_{out}$.

## Conclusion

The output power characteristics of the SR-SAB converter for the output DC voltage variation obtained as simplified equation using four parameters of secondary current. The effectiveness of the output power characteristics of the SR-SAB converter is verified by experiments.

## References


[1] Yu Fang, Songyin Cao, Yong Xie and P. Wheeler, "Study on bidirectional-charger for electric vehicle applied to power dispatching in smart grid," 2016 IEEE 8th International Power Electronics and Motion Control Conference (IPEMC-ECCE Asia), 2016, pp. 2709-2713, doi: 10.1109/IPEMC.2016.7512726.

[2] B. Zhao, Q. Song, W. Liu and Y. Sun, "Overview of Dual-Active-Bridge Isolated Bidirectional DC–DC Converter for High-Frequency-Link Power-Conversion System," in IEEE Transactions on Power Electronics, vol. 29, no. 8, pp. 4091-4106, Aug. 2014, doi: 10.1109/TPEL.2013.2289913.

[3] M. H. Kheraluwala, R. W. Gascoigne, D. M. Divan and E. D. Baumann, "Performance characterization of a high-power dual active bridge dc-to- dc converter", IEEE Trans. Ind. Appl., vol. 28, no. 6, pp. 1294-1301, 1992.

[4] S. Inoue and H. Akagi, "A Bi-Directional DC/DC Converter for an Energy Storage System," APEC 07 - Twenty-Second Annual IEEE Applied Power Electronics Conference and Exposition, 2007, pp. 761-767, doi: 10.1109/APEX.2007.357601.

[5] R. Huang and S. K. Mazumder, "A Soft-Switching Scheme for an Isolated DC/DC Converter With Pulsating DC Output for a Three-Phase High-Frequency-Link PWM Converter," in IEEE Transactions on Power Electronics, vol. 24, no. 10, pp. 2276-2288, Oct. 2009, doi: 10.1109/TPEL.2009.2022755.

[6]G. D. Demetriades and H. P. Nee, "Characterisation of the Soft-switched Single-Active Bridge Topology Employing a Novel Control Scheme for High-power DC-DC Applications," 2005 IEEE 36th Power Electronics Specialists Conference, 2005, pp. 1947-1951, doi: 10.1109/PESC.2005.1581898.

[7] K. Park and Z. Chen, "Analysis and design of a parallel-connected single active bridge DC-DC converter for high-power wind farm applications," 2013 15th European Conference on Power Electronics and Applications (EPE), 2013, pp. 1-10, doi: 10.1109/EPE.2013.6631854.

[8] Ryo Haneda, Hirofumi Akagi and Kenji Hukuda, "Output Voltage Regulation of a Unidirectional Isolated DC-DC Converter Used as an Auxiliary Power Supply for Electric Commuter Trains", IEEJ Trans. IA, vol. 137, no. 5, pp. 406-413, 2017.

[9] C. A. Tuan, H. Naoki and T. Takeshita, "Unidirectional Isolated High-Frequency-Link DC-DC Converter Using Soft-Switching Technique," 2019 IEEE 4th International Future Energy Electronics Conference (IFEEC), 2019, pp. 1-7

[10]Cao Anh Tuan, Takaharu T., “Analysis of Unidirectional Secondary Resonant Single Active Bridge DC-DC converter”, Energies 2021, 14, 6349, 2022, p14

[11] Cao Anh Tuan, Takaharu Takeshita, "Output Power Characteristics of Unidirectional Secondary-Resonant Single-Active-Bridge DC-DC Converter using Pulse Width Control", IEEJ Journal of Industry Applications, Volume 11, Issue 2, pp. 359-368, 2022.